Journal of Solid State Chemistry 184 (2011) 753–763

Contents lists available at ScienceDirect

Journal of Solid State Chemistry

journal homepage: www.elsevier.com/locate/jssc

Thermal low spin–high spin equilibrium of Fe(II) in thiospinels $CuFe_{0.5}(Sn_{(1-x)}Ti_x)_{1.5}S_4$ $(0 \le x \le 1)$

M. Womes [a,*], C. Reibel [a], A. Mari [b], D. Zitoun [a,1]

[a] Université Montpellier II, Institut Charles Gerhardt (UMR CNRS 5253), CC015, Place E. Bataillon, 34095 Montpellier Cedex 5, France
[b] Laboratoire de Chimie de Coordination (UPR CNRS 8241), 205 route de Narbonne, 31077 Toulouse Cedex 04, France

ARTICLE INFO

Article history:
Received 7 September 2010
Received in revised form
20 January 2011
Accepted 31 January 2011
Available online 4 February 2011

Keywords:
Spinel lattice
Spin crossover
Exchange interaction
Magnetic properties
Mössbauer spectroscopy

ABSTRACT

A series of spinel compounds with composition $CuFe_{0.5}(Sn_{(1-x)}Ti_x)_{1.5}S_4$ $(0 \le x \le 1)$ is analysed by X-ray diffraction, measurements of magnetic susceptibilities and ^{57}Fe Mössbauer spectroscopy. All samples show a temperature-dependent equilibrium between an electronic low spin $3d(t_{2g})^6(e_g)^0$ and a high spin $3d(t_{2g})^4(e_g)^2$ state of the Fe(II) ions. The spin crossover is of the continuous type and extends over several hundred degrees in all samples. The Sn/Ti ratio influences the thermal equilibrium between the two spin states. Substitution of Sn(IV) by the smaller Ti(IV) ions leads to a more compact crystal lattice, which, in contrast to many metal–organic Fe(II) complexes, does not stabilise the low spin state, but increases the residual high spin fraction for $T \to 0$ K. The role played by antiferromagnetic spin coupling in the stabilisation of the high spin state is discussed. The results are compared with model calculations treating the effect of magnetic interactions on spin state equilibria.

© 2011 Elsevier Inc. All rights reserved.

1. Introduction

According to the energy level diagrams established by Tanabe and Sugano [1] for first row transition elements in octahedral coordination, one expects to find Fe(II) in one of two electronic ground states, depending on the strength of the crystal field Δ, which splits the 3*d* orbitals into a triplet (t_{2g}) and a doublet (e_g). In weak crystal fields, the electronic ground state is given by $3d(t_{2g})^4(e_g)^2$. This electron configuration, characterised by a total electron spin $S=2$, is commonly referred to as high spin state (HS, $^5T_2$). In strong crystal fields, a $3d(t_{2g})^6(e_g)^0$ ground state characterised by $S=0$ is encountered, commonly referred to as low spin state (LS, $^1A_1$).

In general, the energy difference between the electronic ground state and the first higher lying spin state is so important that spin state transitions cannot be readily induced under laboratory conditions. In some cases, however, the energy difference ΔE_{HL} between the two spin states is sufficiently small that a transition can be induced by externally applied perturbations. Some compounds with a HS ground state can be converted to the LS state under high pressure [2] while other compounds with a LS ground state show a thermally induced crossover to the HS state at temperatures below or around 300 K. Alternatively, the LS to HS transition can be stimulated by irradiation with light or by exposure to strong magnetic fields (see, e.g., the reviews in [3,4]).

Compounds allowing externally induced spin crossover are a field of intensive research since more than fourty years. The perspective to obtain isolated atomic or molecular centres individually switchable from diamagnetic ($S=0$, LS) to paramagnetic ($S=2$, HS) seems to open new ways in the field of data storage.

The numerous compounds showing spin crossover can be classified on the basis of the spatial arrangement and the density of the spin-carrying ions within the crystal lattice. The first class comprises the majority of the metal–organic complexes studied so far: mononuclear complexes, in which a single transition metal ion is present per formula unit. These ions can be considered as single spins embedded in a diamagnetic environment of voluminous organic ligands separating them sufficiently from each other that spin–spin interactions may be neglected. In some dinuclear systems as the next class of compounds the two transition metal ions per formula unit are close enough that exchange interaction between the two spins can lead to magnetic coupling. New phenomena such as two-step spin crossover of the form LS–LS → LS–HS → HS–HS are observed [5–7]. Clusters of spins can be considered as the third class of compounds. Such a case is encountered in the compound Nb_6I_{11} in which clusters of six niobium atoms are interconnected in a three-dimensional framework by bridging iodine–iodine bonds [8]. The last step on the way from mono- to polynuclear systems is accomplished when we finally arrive at inorganic compounds in which the

* Corresponding author. Fax: +33 4 67 14 33 04.
E-mail address: manfred.womes@orange.fr (M. Womes).
[1] Present address: Department of Chemistry and Bar Ilan Institute of Nanotechnology and Advanced Materials (BINA), Bar Ilan University, Ramat Gan 52900, Israel.

0022-4596/$ - see front matter © 2011 Elsevier Inc. All rights reserved.
doi:10.1016/j.jssc.2011.01.038

spin-carrying metals M form a continuous, three-dimensional sublattice and in which they are separated from each other by anions *X* – like O or S – in simple sequences like M–*X*–M. In such lattices, long-ranging magnetic ordering by direct or super-exchange becomes possible. However, corresponding examples exhibiting a LS–HS crossover are extremely scarce compared to the large number of metal–organic complexes. Examples of this kind are the perovskites $La_{1-x}Sr_xCoO_3$ (see, e.g., the review in [9]), the compounds $Fe_xTa_{1-x}S_2$ for $x \leq 1/3$ [10] and the spinels $CuFe_{0.5}Sn_{1.5}S_4$ and $AgFe_{0.5}Sn_{1.5}S_4$ [11].

The unusual magnetic properties of $CuFe_{0.5}Sn_{1.5}S_4$ and $AgFe_{0.5}Sn_{1.5}S_4$ were first investigated by Padiou et al. [12] and were later identified by ^{57}Fe Mössbauer spectroscopy as a spin crossover of iron(II) [11]. In $CuFe_{0.5}Sn_{1.5}S_4$ Cu(I) ions occupy the tetrahedral sites while Fe(II) and Sn(IV) ions are found in random distribution on the octahedral sites of the spinel lattice [13], which will be described in more details in Section 3. The compound is also known as natural mineral rhodostannite [14].

In many cases the cations of a spinel compound can be substituted by cations of another element under conservation of the original lattice structure. In this way, spinels easily form solid solutions with other spinel compounds in any stoichiometric ratio. Frequently, the physical properties of these solid solutions vary continuously with composition from those of one end member to those of the other. A well known example is the linear variation of the lattice parameter described by Vegard's law.

Previous work on $CuFe_{0.5}Sn_{1.5}S_4$ and $AgFe_{0.5}Sn_{1.5}S_4$ has shown that the substitution of Cu(I) by the larger Ag(I) increases – as expected – the lattice constant from 10.33 to 10.58 Å [12]. This lattice expansion has, however, only a weak influence on the thermal equilibrium between HS and LS states. According to the data in [12] the spin transition extends in both compounds over a wide temperature range of several hundred degrees. A purely paramagnetic behaviour of the molar susceptibility χ_m, as described by the Curie–Weiss law:

$$\chi_m = C/(T-\Theta_P) \quad (1)$$

and indicative of a temperature-independent spin state, was observed above approximately 400 K for the copper compound and above 500 K for the silver compound. The values of $\Theta_P = -77$ and -45 K for copper and silver, respectively, indicated an antiferromagnetic interaction between the HS iron ions, which are the only ions in these compounds carrying a magnetic moment.

On the basis of these studies it appeared extremely relevant to examine the effect of a lattice contraction on the thermal spin equilibrium. The recent synthesis of the spinels $CuFe_{0.5}Ti_{1.5}S_4$ [15] and $CuFe_{0.5}Sn_{0.75}Ti_{0.75}S_4$ [16] demonstrated the existence of solid solutions $CuFe_{0.5}(Sn_{(1-x)}Ti_x)_{1.5}S_4$ for $(0 \leq x \leq 1)$. The substitution of Sn(IV) by the smaller Ti(IV) on octahedral sites allows to reduce the lattice constant from 10.33 Å for $x=0$ to 9.999 Å for $x=1$ [15]. The aim of the present work is to present a detailed study of the solid solutions $CuFe_{0.5}(Sn_{(1-x)}Ti_x)_{1.5}S_4$ $(0 \leq x \leq 1)$ with emphasis on the magnetic properties and their dependence on x by combining ^{57}Fe Mössbauer spectroscopy and magnetic measurements.

2. Experimental

A series of samples with general composition $CuFe_{0.5}(Sn_{(1-x)}Ti_x)_{1.5}S_4$ was synthesised by heating stoichiometric mixtures of the elements in evacuated silica ampoules to a temperature of 1023 K for 7 days (S: Fluka, 99.5%; Ti: Merck, ≥98%; Fe: Aldrich, 99.9%; Cu: Merck, ≥99.7%, Sn: Merck, ≥99.8%). X-ray powder diffractograms recorded on a Philips X'Pert diffractometer (Cu*K*α radiation) revealed that the spinel phase was obtained in all cases. Lattice constants were calculated using the POWDER programme. Single crystals of $CuFe_{0.5}Sn_{1.5}S_4$ were grown by transport reaction, using iodine as transport agent (I: Aldrich, 99.8%) [17,18]. 150 mg of sample powder was placed in a silica tube of 20 cm length and 18 mm inner diameter, together with an amount of iodine corresponding to 5 mg/cm^3 tube volume. The evacuated tube was placed in a tubular furnace equipped with two filaments. One extremity of the tube, the powder zone, was heated to 1048 K, the other extremity, the crystallisation zone, was kept at 973 K. These temperatures were maintained for eleven days. Single crystal X-ray diffraction was carried out on an automated Nonius CAD-4 diffractometer (Mo*K*α radiation) at temperatures between 125 and 295 K. The unit cell volume and the lattice parameters of $CuFe_{0.5}Sn_{1.5}S_4$ were determined from 12 selected reflections. These reflections were initially indexed supposing a cubic face-centred lattice with lattice constants $a=b=c$ and angles $\alpha=\beta=\gamma=90^\circ$. The reflections were chosen in the range $-5 \leq (h,k,l) \leq 8$. In a subsequent refinement procedure the parameters a, b, c and α, β, γ were allowed to vary independently around the starting values determined initially for the supposed *cfc* lattice.

Low temperature magnetic susceptibilities were measured on a Superconducting Quantum Interference Design (SQUID) magnetometer MPMS XL7 from 2 K upwards to 300 K after cooling the sample to 2 K under zero-field conditions. High temperature magnetic susceptibilities were measured in a separate run on a different magnetometer MPMS XL7 equipped with an oven from 300 K upwards to 800 K. All measurements were carried out in a magnetic field of 0.5 T.

Mössbauer spectra were recorded in the constant acceleration mode and in transmission geometry on a standard Mössbauer spectrometer composed of components from Ortec and Wissel. A ^{57}Co(Rh) source with a nominal activity of 370 MBq was used. Low temperature spectra were recorded by cooling the sample in a flow cryostat from L'Air Liquide, using liquid nitrogen or liquid helium as cooling agent. The source was always kept at room temperature. The hyperfine parameters isomer shift (δ), hyperfine magnetic field (H), quadrupole splitting (ΔE_q) for $H=0$, and quadrupolar perturbation ($2\varepsilon'$) for $H \neq 0$ as well as the full line-width at half height (2Γ) were determined by fitting Lorentzian lines to the experimental data. Isomer shifts are given with respect to the centre of a room temperature spectrum of α-Fe.

3. Crystal structure

The general composition usually associated with the spinel structure is $(A)[B_2]X_4$ where A and B represent the cations and X the anion. The space group is $Fd\bar{3}m$. The unit cell contains 32 anions X in a cubic close-packed arrangement. Eight cations A per unit cell occupy the tetrahedrally coordinated 8*a* sites, symbolised by round brackets, while sixteen cations B occupy the 16*d* sites in octahedral coordination symbolised by square brackets. Each anion X is bonded to one A and three B cations as shown in Fig. 1. Each B cation is connected to six other B cations via the orbitals of the intermediate anions X. These six B cations represent the second-nearest neighbours of a B cation. In the ideal spinel lattice the atoms B–X–B form an angle of 90°. Each B cation is also connected to six A cations which represent the third-nearest neighbours. The atoms B–X–A form an angle of approximately 125°. The real spinel lattice shows in general some more or less important distortions. Many cations are too large to be accommodated on the interstice between the four anions of an A site. As a consequence, the anions are slightly shifted away from their ideal positions along the four [111] directions of the cube.

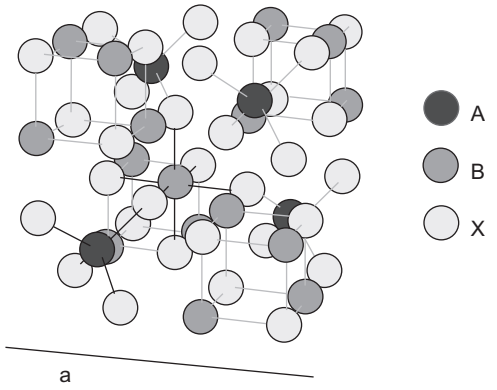

Fig. 1. Schematic view of the spinel structure. The drawing shows a unit cell with 32 anions *X*, 16 *B* cations and the 4 *A* cations situated within the unit cell. Further *A* cations sitting on edges and corners of the unit cell and being shared with adjacent cells were omitted for the sake of clarity. The coordination spheres of one *A* cation and one *B* cation are highlighted by thick solid lines.

This displacement conserves the tetrahedral symmetry of the *A* sites, but produces a weak trigonal distortion of the *B* sites, so that the *B*–*X*–*B* angles slightly deviate from 90°. In the samples under investigation, the tetrahedral *A* (8*a*) sites are filled by Cu(I) ions, while the octahedral *B* (16*d*) sites are occupied by Fe(II), Sn(IV) and Ti(IV) in random distribution.

4. Results and discussion

Fig. 2 shows X-ray powder diffraction patterns of three samples of the $CuFe_{0.5}(Sn_{(1-x)}Ti_x)_{1.5}S_4$ series with $x=0$, 0.5 and 1. The diffraction peaks are indexed in space group $Fd\bar{3}m$. Additional weak reflections at 14.3° for $x=0.5$ or at 13.7° for $x=1$ might indicate the presence of very small amounts of impurities. The variation of the line intensities of the spinel phase with *x*, especially the variation of the (220)/(111) intensity ratio, which depends on the ratio of the scattering factors of the atoms on *B* and *A* sites, and the strong reduction of the (222) and (331) intensities for $x=0.5$, are consistent with a substitution of tin by titanium on the octahedral sites under conservation of the spinel structure. This has been shown by careful Rietveld analysis of the isostructural solid solutions $CuCo_{0.5}(Sn_{(1-x)}Ti_x)_{1.5}S_4$ [19]. Fig. 3 shows the variation of the lattice parameter *a* with composition. The lattice parameter decreases from 10.334(3) Å for $x=0$ to 9.996(2) Å for $x=1$ as expected for the substitution of Sn(IV) with an ionic radius of 0.69 Å by the smaller Ti(IV) with a radius of 0.605 Å [20]. Connecting the data points of the two end members of the series by a straight line shows, however, that the decrease is not linear with *x*, in disagreement with Vegard's law. The lattice parameter deviates towards lower values for all intermediate compositions. We shall return to this point below.

First, we examine in more details the thermal LS–HS equilibrium of Fe(II) in $CuFe_{0.5}Sn_{1.5}S_4$ ($x=0$). The molar susceptibility χ_m of paramagnetic substances is given by

$$\chi_m = N\mu_{eff}^2/3kT \quad (2)$$

where *N* is the Avogadro number, μ_{eff} the effective magnetic moment and *k* the Boltzmann constant. In $CuFe_{0.5}Sn_{1.5}S_4$ the only ion with a non-zero magnetic moment is HS Fe(II), while LS Fe(II) and all other ions are diamagnetic. We may thus replace *N* in Eq. (2) by $N_{(T)}^{HS}$, the number of HS Fe ions per mole, which depends on temperature:

$$\chi_m = N_{(T)}^{HS}\mu_{eff}^2/3kT \quad (3)$$

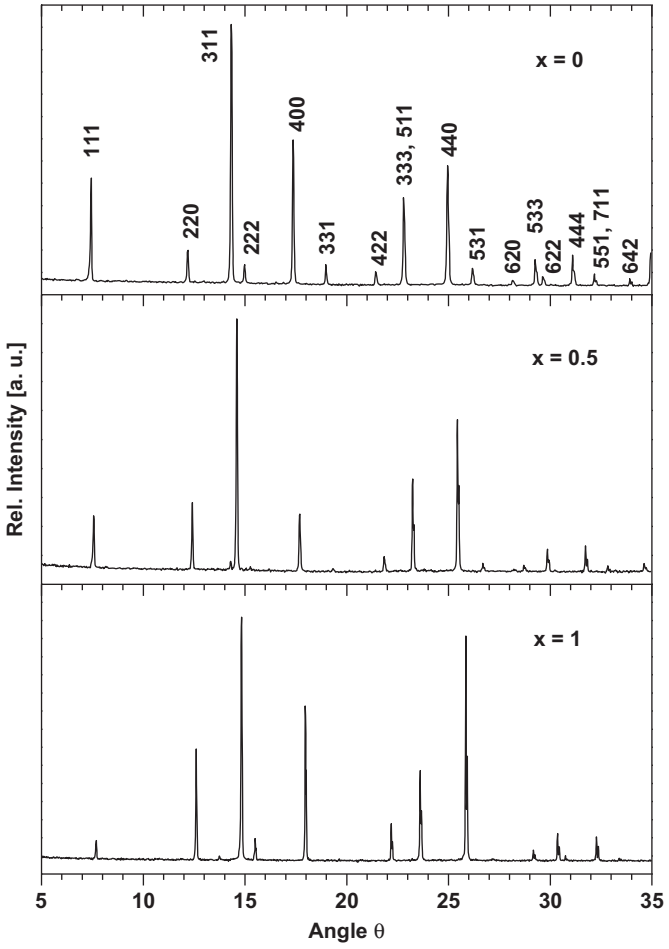

Fig. 2. X-ray diffraction patterns of three samples of the $CuFe_{0.5}(Sn_{(1-x)}Ti_x)_{1.5}S_4$ series with $x=0$, 0.5 and 1. The diffraction peaks are indexed in space group $Fd\bar{3}m$.

This temperature dependence can be visualised by plotting $\chi_m T$ versus *T* as demonstrated by several previous studies [5–7]. Fig. 4a shows such a plot for $CuFe_{0.5}Sn_{1.5}S_4$. The low and high temperature parts of the curve were measured on two different magnetometers, which explains the small offset at 300 K.

These data can now be compared to informations obtained by ^{57}Fe Mössbauer spectroscopy. Fig. 5 shows a series of spectra recorded at various temperatures between 5 and 473 K. The plateau above 550 K in the $\chi_m T$ curve indicates that $N_{(T)}^{HS}$ has reached its maximum value. It may be concluded from the Mössbauer spectra that at this temperature all iron is in the HS state. Hence, according the $\chi_m T$ versus *T* plot, the transition from the LS to the HS state extends over approximately 550 degrees, which is somewhat more than the 400 degrees reported previously in studies based on a rather low number of data points and in which the plateau zone was delimited with less accuracy [11,12]. The point of equal populations of the HS and LS states is reached at $T_{1/2}=210$ K, i.e., at the temperature at which the slope of the curve increases considerably.

Low temperature Mössbauer spectra of $CuFe_{0.5}Sn_{1.5}S_4$ show two doublets the hyperfine parameters of which, given in Table 1, are characteristic for HS and LS iron(II) [21]. The fraction of HS iron derived from these spectra, assuming equal probabilities for recoilless absorption for both HS and LS iron, is also shown in Fig. 4a. The values are in good agreement with the $\chi_m T(T)$ plot with the exception of the data point at 5 K. The steep drop of the $\chi_m T$ values below 20 K is not reproduced by the Mössbauer data. Hysteresis effects can be excluded. Magnetic susceptibilities

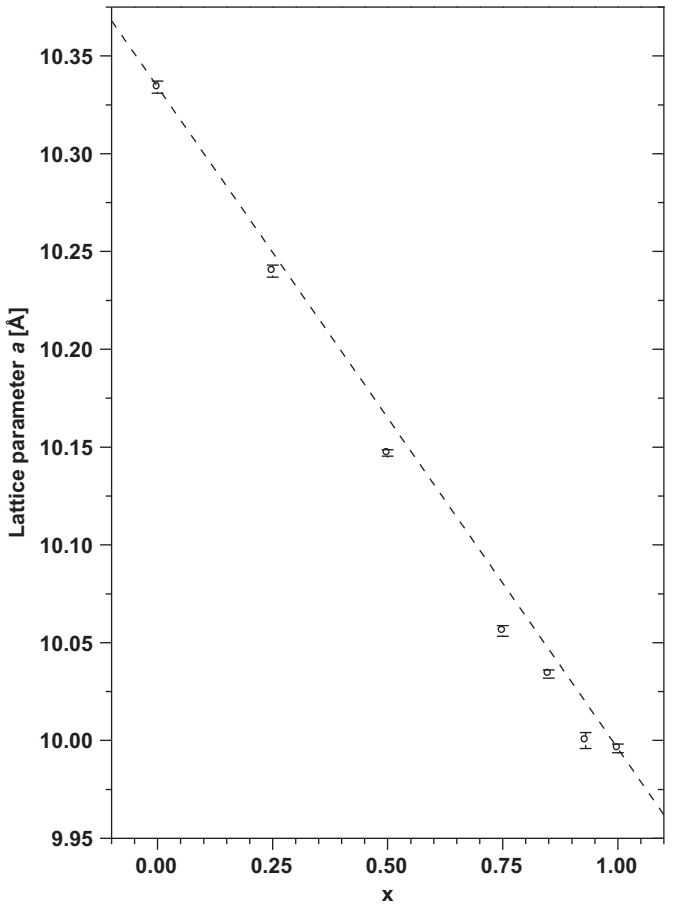

Fig. 3. Variation of the lattice parameter a, calculated in space group $Fd\bar{3}m$, with x in $CuFe_{0.5}(Sn_{(1-x)}Ti_x)_{1.5}S_4$. The dashed line connects the experimental data points of the two end members of the series as expected for a linear decrease according to Vegard's law.

measured from room temperature downwards and from 2 K upwards gave a hysteresis of 2 K at temperatures around 20 K. We therefore ascribe the drop of the susceptibility at low temperatures to zero-field splitting of the spin multiplet of HS iron and the preferred occupation of a low lying level with $M_s=0$. Thus, the conversion to the LS state is not complete at low temperatures. The residual HS fraction at 5 K amounts to 22% according to Mössbauer spectroscopy.

The shape of the Mössbauer spectra recorded at temperatures above 178 K is influenced by a dynamical effect. In this temperature range, the fluctuation rate of iron between HS and LS becomes comparable to or faster than τ^{-1}, the inverse of the lifetime of the excited ^{57}Fe nuclear state ($\tau^{-1}\cong 10^7\ s^{-1}$). As a consequence, the distributions of the electric charges and the electric hyperfine interaction seen by the Mössbauer nucleus become an average of those of the HS and the LS state. The spectral shape reflects this averaging by a merging to one common absorption line of the $\pm 1/2 \rightarrow \pm 1/2$ nuclear transitions of both spin states on one hand side and of the $\pm 1/2 \rightarrow \pm 3/2$ transitions of both spin states on the other hand side [22,23]. When going from low to high temperatures, i.e., when starting at a static situation from the point of view of Mössbauer spectroscopy, the first sign observed of such a dynamical effect is an onsetting line broadening of the still resolved HS and LS doublets. A further increase of the temperature leads to time-averaged spectra in which the two spin states become undistinguishable by Mössbauer spectroscopy. Finally, above 400 K, when the HS fraction becomes more and more predominant, the spectral shape evolves to that of a single doublet from HS iron. The spectral shape observed for $x=0$ between 220 and 473 K agrees well with simulations of such a dynamical effect by Adler et al. [23].

Fig. 4b shows the evolution of the unit cell volume, determined by single crystal X-ray diffraction in the temperature range from 125 to 295 K. The data reveal a change in the slope, occurring around 210 K, with a stronger volume expansion for $T>210$ K, i.e., in the same temperature range where the $\chi_m T$ versus T plot in Fig. 4a indicates an enhanced conversion of Fe(II) to the HS state. It is known from complexes containing Fe(III) in six-fold sulphur coordination that the Fe–S bond length increases by 0.05–0.1 Å when the metal ion changes from the LS to the HS state [24]. The enhanced volume expansion above 210 K is thus correlated with the enhanced conversion of iron to the HS state.

A first determination of the lattice parameters was made supposing a cubic face-centred lattice, i.e., using the constraints $\alpha=\beta=\gamma=90^\circ$ and $a=b=c$. In a subsequent refinement procedure, these parameters were allowed to vary independently, using the result of the first step as the starting values for the refinement. In this refinement the angles α, β and γ between the lattice axes remained at a constant value of $(90.00\pm0.02)^\circ$ at all temperatures between 125 and 293 K. The evolution of the lattice parameters a, b and c in this temperature range is shown in Fig. 4c. The data reveal a weak orthorhombic distortion of the cubic unit cell with $a<b<c$ at all temperatures. This distortion becomes strongest at 190 K, while at 210 K the weakest distortion with an almost perfect cubic unit cell is observed. Comparison with the $\chi_m T(T)$ plot shows that, at $T=190$ K, about 45% of the iron atoms are in the HS state while the point of minimal distortion coincides with $T_{1/2}=210$ K. At temperatures above 210 K a tendency towards a weak tetragonal distortion with $b=a$ is observed, while at low temperatures the lattice seems to evolve towards a tetragonal distortion with $b=c$.

The following scenario could explain these observations. At temperatures well below 210 K the majority of iron is in the LS state. The lattice structure is determined by the shape of the $Fe(II)_{LS}$–S_6 polyhedra. HS iron atoms can be considered as being isolated from each other within this lattice due to their low concentration, representing a local distortion of the lattice by their longer Fe–S bond lengths. As the fraction of HS iron increases $Fe(II)_{HS}$–S_6 polyhedra are no longer a local and isolated distortion but induce now a collective and static distortion as it is seen by XRD at 190 K with 45% HS iron. At $T_{1/2}=210$ K, where Mössbauer spectroscopy indicates a rapid fluctuation between the two spin states, the lattice distortion becomes dynamic and the average distortion seen by XRD vanishes. At higher temperatures, when the HS fraction becomes more and more predominant, XRD shows again a static lattice distortion, now with a tendency towards $b=a$ in contrast to the $b=c$ tendency of the LS dominated lattice. It was already emphasised that an enhanced conversion to the HS state can be observed above the point of equal spin state populations. It can be concluded that the HS dominated lattice above $T_{1/2}$ facilitates the transition from the LS to the HS state by lowering the activation energy.

We turn now to the influence of the Sn/Ti substitution on the thermal spin equilibrium. Fig. 6 shows plots of $\chi_m T$ versus T for various values of x. The left panel shows the data for $x=0$, 0.25 and 0.5 while the right panel shows those for $x=0.5$, 0.75, 0.85, 0.93 and 1. For $x=0.25$ and 0.5, the $\chi_m T$ curves follow closely that of $x=0$ at low temperatures, but do not show the same change in slope around 200 K. Instead, the curves show a rather linear increase over a wide temperature range extending from approximately 130 to 360 K for $x=0.25$ and from 150 to 300 K for $x=0.5$. The conversion to the HS state is completed at higher temperatures than for $x=0$, at approximately 700 K for both compounds. When x is raised from 0.5 to 1, the shape of the $\chi_m T$ versus T plots

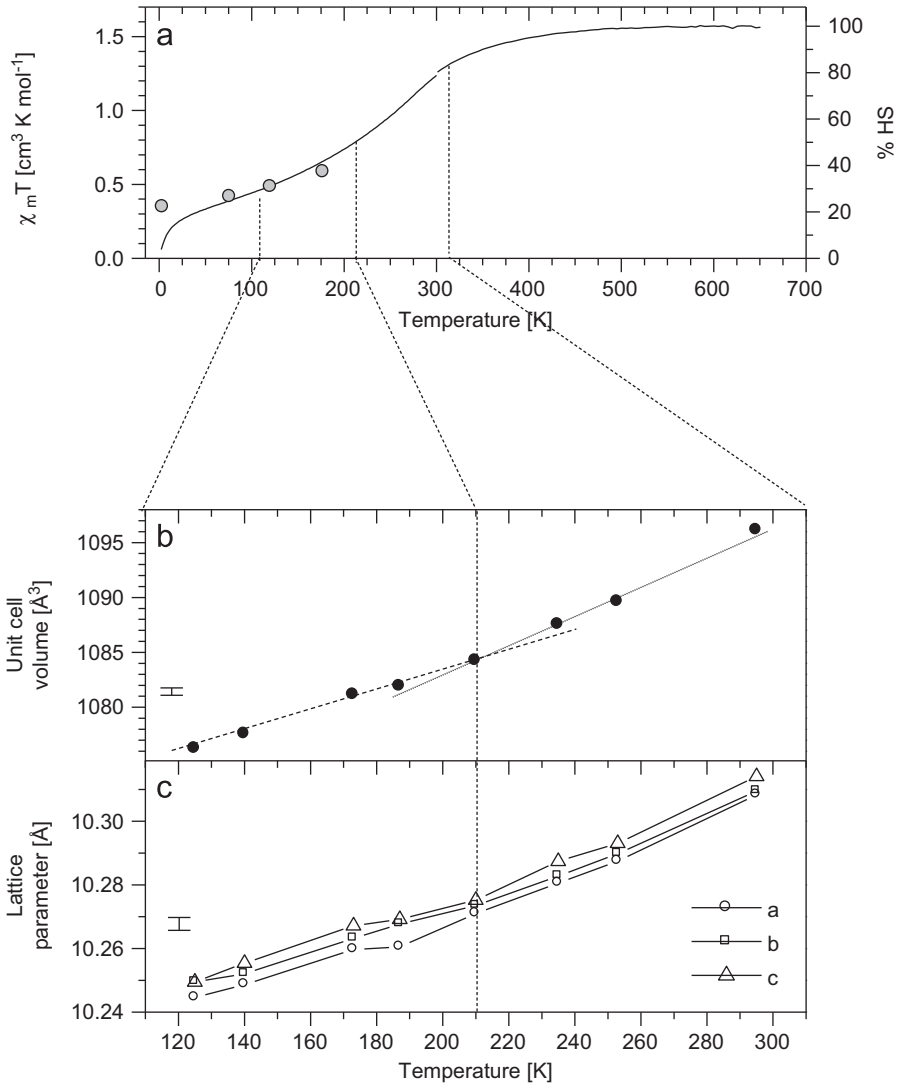

Fig. 4. (a) Molar susceptibility χ_m of $CuFe_{0.5}Sn_{1.5}S_4$, plotted as $\chi_m T$ versus T (dots, left axis of ordinates). Comparison with the fraction of HS iron derived from ^{57}Fe Mössbauer spectra (circles, right ordinate), (b) temperature variation of the lattice volume of $CuFe_{0.5}Sn_{1.5}S_4$ determined by single crystal X-ray diffraction, dashed and dotted lines are guide lines for the eye (experimental errors are less than 0.6 Å^3, the error bar indicates the maximum error), (c) temperature variation of the lattice parameters of $CuFe_{0.5}Sn_{1.5}S_4$ determined by single crystal X-ray diffraction (experimental errors are less than 0.004 Å, the error bar indicates the maximum experimental error).

changes from a rather linear ascent for $x=0.5$ to a curved shape for $x=1$. The temperature at which a constant value is reached decreases somewhat from approximately 700 K for $x=0.5$ to 600 K for $x=1$. The inset in Fig. 6 shows plots of the inverse of the molar susceptibility versus temperature for $x=0.85$, 0.93 and 1. They reveal an antiferromagnetic long-range order in these three compounds with Néel temperatures T_N of 4, 5 and 7 K, respectively. The data for $x=0.75$ (not shown) suggest equally the occurrence of such a long-range order with a T_N below 2 K. Assuming the validity of a Curie–Weiss law as described by Eq. (1) in the region of constant $\chi_m T$ values, the parameters Θ_P and μ_{eff} were determined for all samples from linear fits to the data points. All effective magnetic moments lie close to the spin-only value of $4.90\mu_{eff}$ (see Table 2). Negative values of Θ_P were obtained for all samples, indicating antiferromagnetic spin interactions throughout the series. The low value of $\Theta_P=-13$ K obtained for $x=0$ shows that spin interactions in this compound are very weak and that the spins of HS iron may be considered as magnetically dilute, which is the basic condition for the application of Eq. (3). The present values of Θ_P and μ_{eff} for $x=0$ differ somewhat from those reported previously ($\Theta_P=-77$ K; $\mu_{eff}=5.31\mu_B$ [12]) which might be due to the low number of data points used in these studies, resulting in a lower accuracy, as already mentioned above.

For $x=0.5$, a series of Mössbauer spectra was recorded at various temperatures between 5 and 295 K. In a first attempt, the spectrum at 5 K was fitted by one doublet for each of the two spin states, as shown in Fig. 7. This fit gives the hyperfine parameters shown in Table 1. Comparison with the corresponding spectrum of $x=0$ shows that both the fraction of residual HS iron and the linewidths 2Γ of LS and HS iron are considerably higher for $x=0.5$ than for $x=0$. At higher temperatures the HS resonance lines show a splitting into several sub-spectra as can be seen from the series of spectra shown in Fig. 8a. The increased linewidth and the line splitting can be understood by considering the local environment of iron in these spinels. The distortion of the octahedral sites responsible for the quadrupole splitting is mainly caused by the *A* cations, as outlined in Section 3. An additional distortion of the charge distribution around the iron nucleus is induced by the six surrounding *B* cations [25]. They influence the exact position of the anions by their respective radii. The direct coulombic contribution to the electric field gradient by the charges on the S^{2-} anions is, however, expected to be rather small. The main

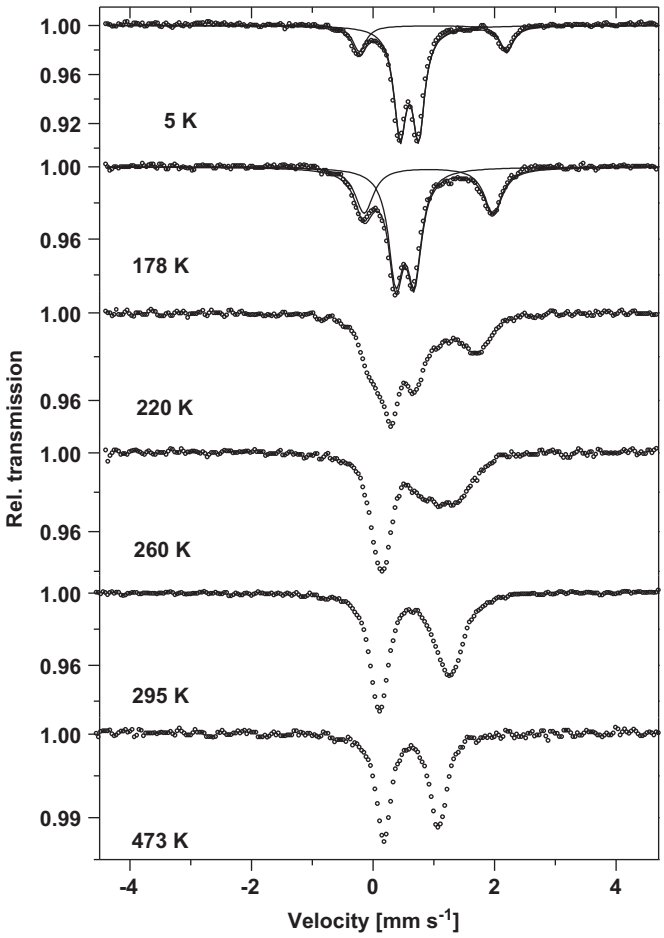

Fig. 5. ^{57}Fe Mössbauer spectra recorded at various temperatures for $x=0$.

Table 1
^{57}Fe hyperfine parameters of the HS and LS state in $CuFe_{0.5}(Sn_{(1-x)}Ti_x)_{1.5}S_4$ at 5 K. Isomer shift (δ), quadrupole splitting (ΔE_q), quadrupolar perturbation ($2\varepsilon'$) and full linewidth at half maximum (2Γ) in mm s^{-1}, contribution to total absorption (C) in %.

	HS				LS			
x	δ	ΔE_q	2Γ	C	δ	ΔE_q	2Γ	C
0	0.99(1)	2.42(1)	0.27(1)	22(2)	0.60(1)	0.31(1)	0.24(1)	78(2)
0.5	0.87(1)	2.26(1)	0.52(2)	34(2)	0.60(1)	0.54(1)	0.41(1)	66(2)
0.75	0.86(1)	2.05(1)	0.54(2)	39(2)	0.61(1)	0.55(1)	0.43(1)	61(2)
0.85	–[a]	–[a]	–[a]	–[a]	0.59(1)	0.52(1)	0.39(1)	–[a]
0.85[b]	0.83(1)	2.00(2)	0.61(2)	42(2)	0.60(1)	0.53(1)	0.39(1)	58(2)
1.0	0.84(9)	0.12(9)[c]	3.4(3)	84(8)	0.55(3)	0.44(6)	0.86(12)	16(8)
1.0[d]	0.84(1)	1.70(1)	0.53(1)	75(2)	0.63(1)	0.52(2)	0.50(3)	25(2)

[a] Parameter not determined, see explanation in the text.
[b] Spectrum recorded above T_N at 9 K.
[c] Quadrupolar perturbation $2\varepsilon'$. Hyperfine magnetic field $H=(18\pm1)T$.
[d] Spectrum recorded above T_N at 14 K.

contribution to the electric field gradient of HS Fe(II) comes from its valence electrons. A first electronic contribution is caused by the $3d(t_{2g})^4$ electron configuration which produces an aspherical charge distribution when the local symmetry is less than cubic [26]. The trigonal field component of spinel B sites splits the t_{2g} states into a singlet and a doublet [27] with the fourth t_{2g} electron occupying at $T=0$ K the lowest of the t_{2g} levels. With increasing temperature the electron populations of the t_{2g} states become more and more balanced as this electron is excited to the first higher-lying state. The time the electron spends in either the ground or the excited level is much shorter than the lifetime of the excited nuclear state, so that the ^{57}Fe nucleus sees only time-averaged level populations resulting in time-averaged quadrupole splittings. We expect therefore a large quadrupole splitting $\Delta E_{q,HS}$ at low temperatures, when this electron occupies the ground state, and a smaller splitting for more balanced populations at higher temperatures. Distortions induced by the B cations can modify the energy difference between the lowest and the first higher-lying electronic state and thus the temperature dependence of $\Delta E_{q,HS}$ [26]. In contrast to $\Delta E_{q,HS}$ no strong temperature dependence is observed for $\Delta E_{q,LS}$ due to the filled $3d(t_{2g})$ subshell of LS Fe(II).

A second electronic contribution to the total quadrupole splitting is induced by unbalanced populations within all $3d$ and $4p$ valence orbitals involved in σ- and π-bonds with sulphur [28]. The charge density in the Fe–S bonds depends on the ionic or covalent character of the competing S–B bonds in the Fe–S_6–B_6 cluster. The S–B bond properties are determined by the radius, the charge and the electronegativity of the B cations. According to Pauling's table of electronegativities, Sn (1.8) and Fe (1.8) can be considered as equivalent while Ti (1.5) is less electronegative. Random distributions of these ions on B sites could therefore lead to different electron occupancies within the bonds of a FeS_6 polyhedron. Calculations show that contributions to the total quadrupole splitting exceeding the total natural linewidth $2\Gamma=0.19$ mm s^{-1} of ^{57}Fe can be produced by differences in the $4p$ populations of less than 0.12 electrons or of less than 0.06 $3d$ electrons. In contrast to the first, this second electronic effect should have only a weak temperature dependence, but it affects the spectra of both HS and LS iron.

Looking at the spectra of $x=0$ between 5 and 178 K, we find low linewidths for both HS and LS iron and no splitting into several HS doublets up to 178 K. Apparently, the geometric effect due to the different radii of Sn(IV) and LS and HS Fe(II) ions on neighbouring B sites is negligible, the level splitting between ground and first excited level of the fourth t_{2g} electron depends only weakly or not at all on the arrangement of these ions, and no additional unbalance in valence orbital populations is induced by the different B cations in the competing S–B bonds. For $x=0.5$ the partial substitution of Sn(IV) by Ti(IV) in a 1:1 ratio increases considerably the number and the probabilities of inhomogeneous environments composed of different ions on B sites and increases thus also the number of theoretically occurring quadrupole splittings, especially if we take into account that different arrangements of a given set of ions (e.g., cis or trans arrangements of two ions of the same kind) lead to different splittings. The increased linewidth already at 5 K points towards a geometric effect by different radii or to unbalanced level populations by different electronegativities of the B cations, or a combination of both. However, no individual HS sub-spectra can be distinguished. The hyperfine parameters in Table 1, resulting from a two-doublet fit, are thus to be considered as an average of a large number of environments. At 180 K the splitting of the HS sub-spectrum into several doublets becomes clearly visible, indicating that the partial Sn/Ti substitution affects also the level splitting between ground and first excited level of the fourth t_{2g} electron. We see no possibility to fit this spectrum with one doublet for each of the theoretically occurring environments and to ascribe them to a given coordination shell without any ambiguity. In order to determine, despite this difficulty, the temperature dependence of the HS:LS ratio from the Mössbauer spectra, which is the most important information for the purposes of this paper, we considered the spectrum recorded at 295 K and found that the spectral shape of the HS part can be reproduced satisfactorily by three doublets. This fitting procedure was then applied to the whole series of spectra, as shown in Fig. 8a, with the aim to

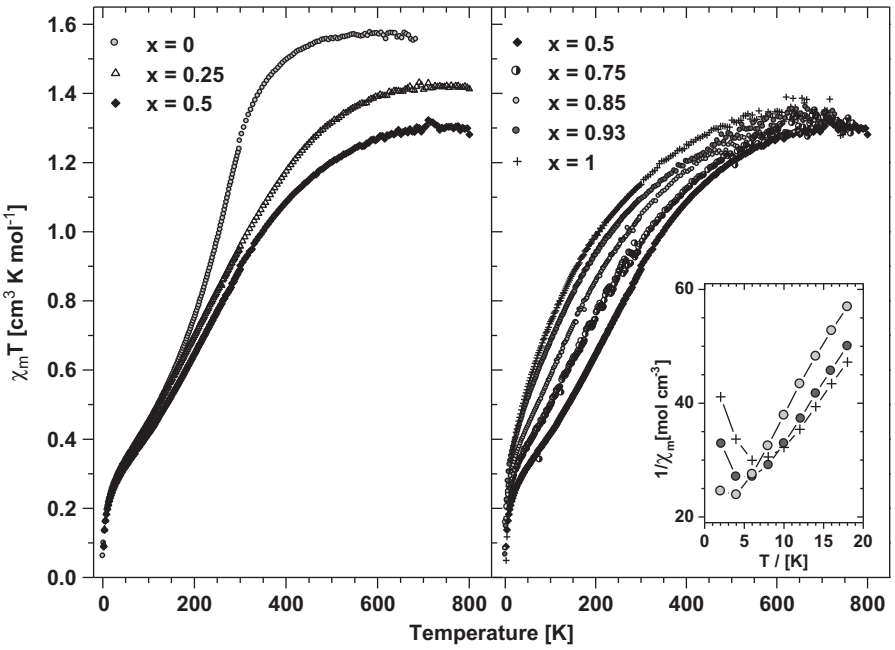

Fig. 6. Temperature dependence of the molar susceptibility χ_m, plotted as $\chi_m T$ versus T for various values of x in $CuFe_{0.5}(Sn_{(1-x)}Ti_x)_{1.5}S_4$. Inset: inverse molar susceptibility plotted versus T for $x=0.85$, 0.93 and 1.

Table 2
Magnetic properties of $CuFe_{0.5}(Sn_{(1-x)}Ti_x)_{1.5}S_4$. T_N: antiferromagnetic Néel temperature; Θ_P: paramagnetic Néel temperature; μ_{eff}: effective magnetic moment.

x	T_N (K)	Θ_P (K)	μ_{eff} (μ_B)
0	–	-13 ± 4	5.09 ± 0.02
0.25	–	-43 ± 7	4.92 ± 0.03
0.5	–	-58 ± 12	4.77 ± 0.04
0.75	<2	-87 ± 42	4.89 ± 0.13
0.85	4 ± 1	-102 ± 35	4.94 ± 0.12
0.93	5 ± 1	-108 ± 21	5.01 ± 0.07
1.0	7 ± 1	-106 ± 35	5.08 ± 0.16

determine this HS:LS ratio for all temperatures from the spectral areas. These three HS sub-spectra are not correlated with any given arrangement of ions and, therefore, the hyperfine parameters obtained from these fits are not published here. Instead, we prefer to restrict the data in Table 1 to the hyperfine parameters from the two-doublet fit at 5 K which demonstrate that the two sub-spectra are effectively due to HS and LS Fe(II). At 5 K the HS:LS ratio of (66 ± 2):(34 ± 2) determined by the two-doublet fitting procedure shown in Fig. 7 and given in Table 1 agrees within experimental uncertainty with the (68 ± 1):(32 ± 1) ratio derived from that same spectrum by the multi-doublet fit shown in Fig. 8a.

For $x=0.5$ the spectral shape of both the HS and LS doublets is not influenced by rapid fluctuations between different spin states and both states can be distinguished at all temperatures up to 295 K. Moreover, the hyperfine parameters of both spin states show a continuous variation with temperature between 5 and 295 K and give no indication of a structural change at $T_{1/2}$ which, according to Mössbauer spectroscopy, is situated between 120 and 180 K. The HS fractions determined from the fits shown in Fig. 8a are plotted in Fig. 8b versus temperature together with the corresponding $\chi_m T$ data. The values from both techniques agree well in the range 220–295 K. Below that range, the Mössbauer HS fraction deviates more and more from the $\chi_m T$ curve as the temperature is lowered.

For $x=0.75$, only a low-temperature Mössbauer spectrum was recorded with the aim to determine the residual HS fraction

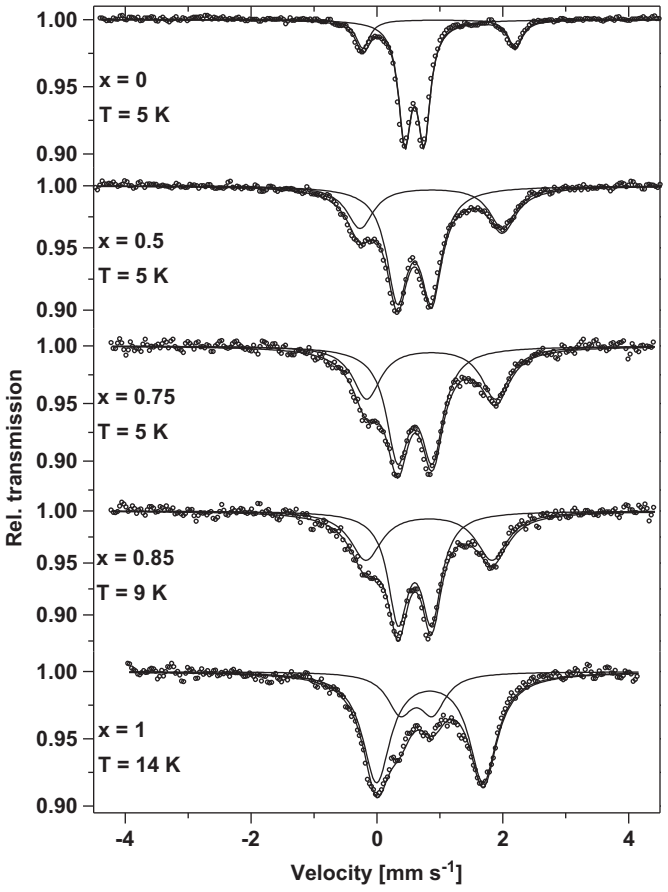

Fig. 7. Low-temperature Mössbauer spectra recorded for samples of the series $CuFe_{0.5}(Sn_{(1-x)}Ti_x)_{1.5}S_4$. Spectra recorded at 5 K for $x=0$, 0.5, 0.75, at 9 K for $x=0.85$, at 14 K for $x=1$.

at 5 K. The spectrum shown in Fig. 7 and the parameters shown in Table 1 reveal that this fraction has further increased with respect to $x=0.5$. The spectrum recorded at 5 K for $x=0.85$,

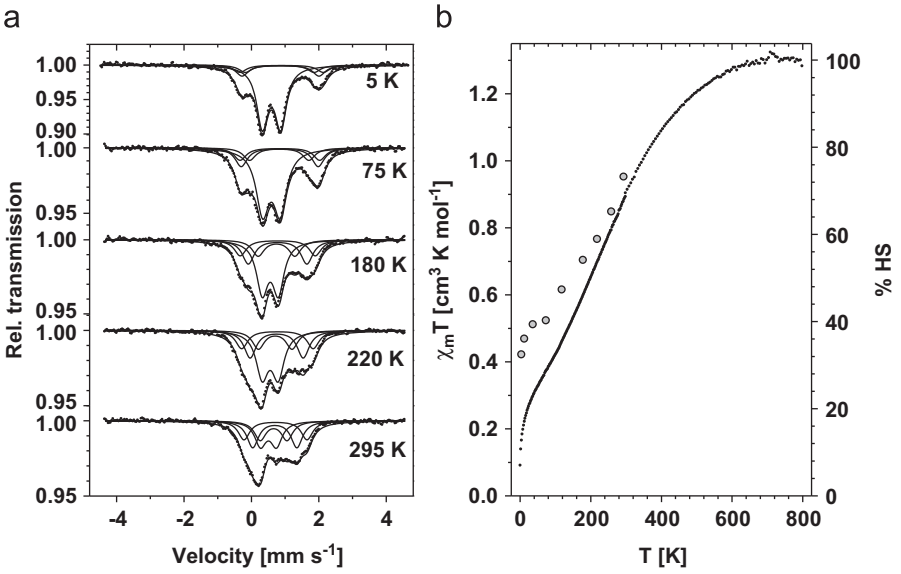

Fig. 8. (a) ^{57}Fe Mössbauer spectra recorded at various temperatures for $x=0.5$, (b) molar susceptibility χ_m for $x=0.5$ plotted as $\chi_m T$ versus T (dots, left axis of ordinates). Comparison with the fraction of HS iron derived from ^{57}Fe Mössbauer spectra (circles, right ordinate).

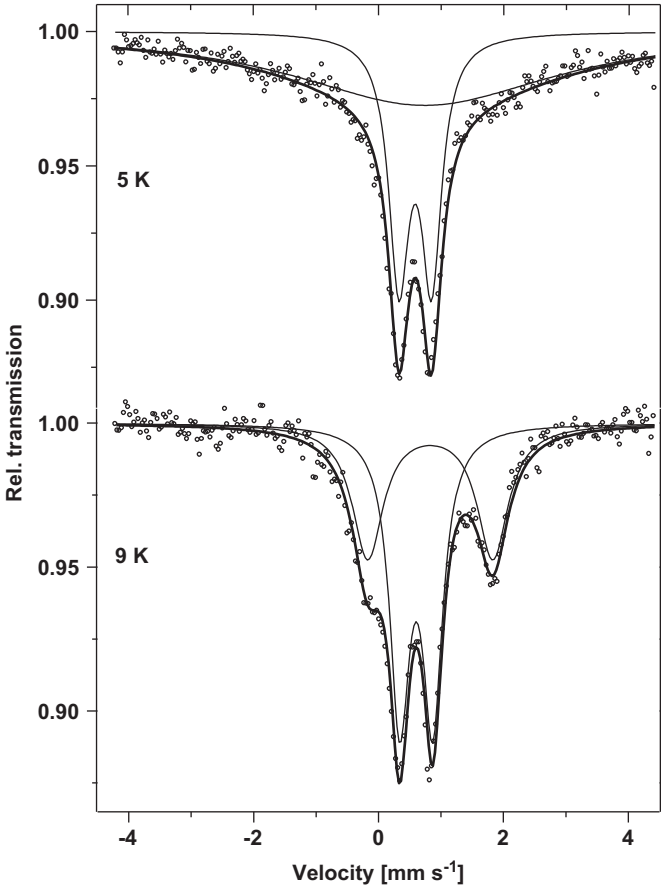

Fig. 9. ^{57}Fe Mössbauer spectra recorded at 5 and 9 K for $x=0.85$.

shown in Fig. 9, shows the characteristic doublet of LS iron while for HS iron no sharp resonance lines can be observed. The temperature of 5 K lies near the Néel temperature of this compound, determined by susceptibility measurements as $T_N=(4\pm1)$ K (Table 2), and thus in the domain of beginning static long-range ordering of the spins of HS iron. In this domain, the spectrum evolves from a doublet of paramagnetic iron to a shape determined by the Zeeman splitting of the nuclear levels in the local static magnetic field and the splitting caused by the electric quadrupolar interaction. Due to the random distribution of magnetic Fe(II) HS and diamagnetic Fe(II) LS, Sn(IV) and Ti(IV) the evolution from the paramagnetic to the magnetically ordered state is likely to proceed differently with temperature for different iron sites, so that no sharp resonance lines of paramagnetic or magnetically ordered iron are observed for HS iron in the vicinity of T_N, making the exact determination of a HS fraction rather difficult. LS iron carries no magnetic moment and no spin–spin interaction occurs with neighbouring ions. Its electrons produce no local magnetic field and the field eventually produced by neighbouring HS iron ions is sufficiently weak on the site of LS iron to have no observable influence on the shape of its doublet. The hyperfine parameters of LS iron at 5 K can be found in Table 1. A second spectrum was recorded above T_N, at 9 K, which is also shown in Fig. 9. Here, HS iron can be identified by its characteristic doublet and the residual HS fraction given in Table 1 was determined from this spectrum.

A series of spectra recorded for $x=1$ at various temperatures is shown in Fig. 10a. At 5 K, below T_N, the sub-spectrum of HS iron shows a strong broadening over a wide velocity range which reflects the Zeeman splitting of the resonance lines in the static magnetic field induced by long-range spin ordering. However, the spectral shape allows no individual resonance lines to be distinguished. The random distribution of magnetic HS Fe(II) ions and non-magnetic LS Fe(II) and Ti(IV) ions on the six nearest B sites allows several environments differing by their number of magnetic neighbours, hence also differing by the intensity of the local magnetic field which, in turn, determines the spectral line splitting. When fitting this broad structure by a single six-line spectrum, as shown in Fig. 10a, we find an isomer shift of 0.83 mm s^{-1} which is characteristic of HS Fe(II). The magnetic field of 18 T should be considered as a rough determination of the average field strength on HS iron sites. The hyperfine parameters of the LS sub-spectrum agree, when fitted with a single doublet, within experimental error with the values found for LS iron in other samples of the series. We observe, however, a strongly increased linewidth as compared to a spectrum of that same sample recorded above T_N at 14 K (see Table 1). While the

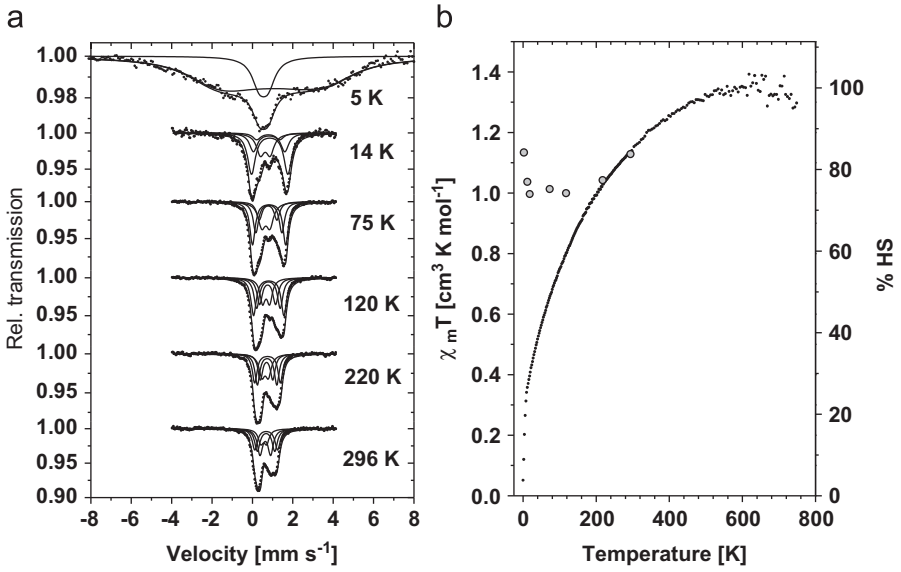

Fig. 10. (a) ^{57}Fe Mössbauer spectra recorded at various temperatures for $x=1$, (b) molar susceptibility χ_m for $x=1$ plotted as $\chi_m T$ versus T (dots, left axis of ordinates). Comparison with the fraction of HS iron derived from ^{57}Fe Mössbauer spectra (circles, right ordinate).

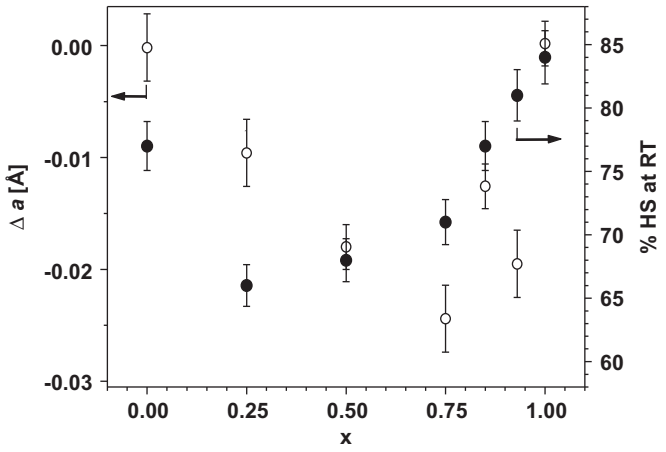

Fig. 11. Plot of the difference Δa between experimental lattice parameters and the linear variation expected from Vegard's law (dashed line in Fig. 3) versus x. Comparison with the fraction of HS iron at room temperature derived from susceptibility data.

linewidth at 14 K can be explained by the variety of possible environments, the additional broadening at 5 K must be due to another phenomenon. A weak static magnetic field on the LS iron sites originating from HS ions would induce an additional splitting of the nuclear levels and thus an additional broadening of the LS sub-spectrum. In this case a fitting procedure taking into account magnetic level splitting would be a more appropriate approach than the doublet used here. However, the fact that no individual resonance lines can be distinguished in this part of the spectrum, even when recorded on a reduced velocity scale, prevents an appropriate fitting. The spectra recorded between 14 and 295 K show no magnetic splitting and give no indication of rapid fluctuations between different spin states or a structural change. The spectrum at 14 K, i.e., above T_N, was fitted by two doublets, as shown in Fig. 7, in order to determine the hyperfine parameters of both spin states with higher precision on a reduced velocity scale. These parameters are also given in Table 1. At higher temperatures the HS resonance lines show a splitting into several sub-spectra. This, together with the considerable linewidth at 14 K, shows that the random distribution of HS Fe(II) and the much smaller Ti(IV) on nearest B sites causes a geometric effect by their different radii or induces unbalanced level populations by their different electronegativities or cause a combination of both effects. As for $x=0.5$ at least three doublets are necessary to reproduce the spectral shape of the HS part satisfactorily, as shown in Fig. 10a. At 14 K, the HS:LS ratio of (75 ± 2):(25 ± 2) determined by the two-doublet fitting procedure shown in Fig. 7 agrees within experimental uncertainty with the (77 ± 2):(23 ± 2) ratio derived from the multi-doublet fit shown in Fig. 10a. The HS fractions determined from these multi-doublet fits are compared in Fig. 10b with a plot of $\chi_m T$ versus T. The values from both techniques agree well in the range 260–295 K. Below that range, the Mössbauer HS fraction remains at a constant level of 75% with the exception of the spectrum recorded at 5 K which will be discussed below.

Figs. 8b and 10b show that at room temperature the HS fractions determined from susceptibility data for $x=0.5$ and 1 agree with those derived from Mössbauer spectra. They can thus be considered as the correct HS fractions and it may be supposed that for all other values of x the magnetic susceptibilities also give the correct HS fractions at room temperature. A plot of these fractions versus x is shown in Fig. 11. The highest values are found for the end members of the series at $x=0$ and 1 while samples around $x=0.5$ show the lowest values. Fig. 11 compares these data with the deviation of the room temperature lattice parameters from the linear decrease with x expected from Vegard's law. These deviations show the same U-shaped dependency on x as the room temperature HS fractions. A lower HS fraction should lead to a lower lattice constant due to the shorter Fe–S bonds in the LS state and the deviation from Vegard's law might thus be due to the variation with x of the amounts of HS iron present in the samples at room temperature.

Below room temperature, we observe a discrepancy between the HS fractions from susceptibility and Mössbauer data which increases with x. Mössbauer spectra recorded at 5 K seem to indicate that substitution of Sn by Ti shifts the thermal equilibrium between the two spin states towards the HS configuration. The substitution of Sn(IV) by Ti(IV) reduces the lattice constant and leads to a closer packing of the anions in the lattice, which also affects the Fe–S bonds by reducing their bond length and by

enhancing their covalent character. This enhanced covalency is reflected by the lower isomer shift δ_{HS} at 5 K for $x=0.5$ and 1 as compared to $x=0$ (see Table 1). A reduction of the Fe–S bond length by ion substitution can be expected to have the same effect as the application of external pressure. The work of Bargeron et al. [2] and many other similar studies have shown that external pressure shifts the spin equilibrium towards the LS state, which is generally seen as a consequence of the shorter metal–ligand bonds in the LS configuration. This is, however, the opposite of what is observed here. Apparently, in the present case a corresponding effect is overcompensated by another phenomenon.

It can be noted that the discrepancy observed between the HS fractions from susceptibility and Mössbauer data below room temperature is correlated with the strength of the antiferromagnetic coupling between the spins of HS Fe(II). For $x=0$, where the low value of $\Theta_P=-13$ K indicates a very weak antiferromagnetic coupling, the susceptibility data agree well with those from Mössbauer spectroscopy (Fig. 4a). The discrepancy increases with x (Figs. 8b and 10b) as the values of T_N increase and those of Θ_P decrease (Table 2) and becomes strongest for $x=1$ where a spontaneous magnetisation occurs below $T_N=7$ K. We thus attribute the discrepancy between HS fractions from susceptibility and Mössbauer data to an onsetting antiparallel ordering of electron spins of neighbouring HS iron ions as a result of a negative exchange interaction between magnetic orbitals (i.e., orbitals occupied by electrons with unpaired spins). The reduced Fe–S bond length in the Ti-substituted samples leads to a stronger overlap between magnetic cation 3*d* and anion p orbitals and to an enhanced negative exchange interaction between 3*d* electrons of neighbouring iron ions via the anion orbitals. In addition, the more compact lattice reduces also the Fe–Fe distance and direct overlap between magnetic 3*d* t_{2g} orbitals of two HS Fe ions might become possible, which also leads to a negative exchange interaction. In both cases μ_{eff}, the average magnetic moment per HS iron ion in Eq. (3), becomes temperature-dependant due to the formation of pairs of HS ions with a total spin $S=0$ and Eq. (3), which is valid only for magnetically dilute systems without magnetic interactions between ions, is no longer applicable for the determination of the fraction of HS iron. The HS fractions derived from Mössbauer spectra are not affected by such spin pairing and remain reliable.

The exchange interaction between magnetic 3*d* orbitals of neighbouring HS ions is a stabilising factor which lowers the free energy of the HS state with respect to that of the LS configuration. This is demonstrated by the correlation between the strength of the antiferromagnetic coupling and the residual HS fraction at low temperatures. The amount of residual HS iron can also be correlated with the number of magnetic neighbours around an iron ion assuming a statistical distribution of Sn, Ti, Fe LS and Fe HS within the spinel lattice. For $x=1$, the probability p_{dia} that iron is surrounded exclusively by diamagnetic Ti(IV) on the six nearest *B* sites is $p_{dia}=0.18$. These iron ions have no possibility to stabilise the HS state by exchange interactions so that $1-p_{dia}=0.82$ should represent the upper limit for the residual HS fraction in these spinels. Mössbauer spectroscopy has shown that for $x=1$ the HS fraction remains at a constant value of 75% between 14 and 220 K. Taking into account the presence of 25% diamagnetic Fe(II) LS in addition to Ti(IV), the probability p_{dia} of an exclusively diamagnetic environment – composed of Fe(II) LS and Ti(IV) – becomes $p_{dia}=0.29$ which gives a residual HS fraction of $1-p_{dia}=0.71$, in good agreement with Mössbauer data. Corresponding calculations for other samples of the series give also a quite satisfying agreement between $1-p_{dia}$ and the experimental residual HS fraction, as shown in Fig. 12.

Our results confirm predictions of a model of LS–HS transitions initially developed by Chestnut [29] and extended by Bari and Sivardière [30] by inclusion of magnetic interactions between neighbouring HS ions. According to this model the Hamiltonian of N ions with a d^6 configuration can be written as

$$H = H_{elast.} + \Sigma_i H_\Delta n_i - \Sigma_{ij} J_{ij} n_i n_j S_i S_j \quad (4)$$

The first term describes the total elastic energy required for the stretching of the cation–anion bonds as it accompanies the LS–HS crossover. The second term represents the energy difference ΔE_{HL} between HS and LS state, with the zero energy corresponding to the LS state. The spin state of the *i*th ion is described by n_i, which takes the values of zero for LS and of one for HS ions. The last term describes the interaction between the spins *S* of two neighbouring ions *i* and *j* with J_{ij} representing the exchange coupling constant. It is obvious that this last term vanishes if one or both ions *i* and *j* are in the LS state. Bari and Sivardière discuss the solutions in terms of the magnitude of *J*. From this follows that low values of *J* (weak coupling) should lead to a thermal population of the HS state without magnetic ordering, as observed in the present work for $x \leq 0.5$. High values of *J* (strong coupling) should lead to a magnetically ordered ground state the magnetisation of which vanishes at a second order transition temperature, as observed in the present case for $x \geq 0.75$. For intermediate values of J the model predicts a non-magnetic LS ground state which transforms at higher temperatures to an ordered HS state the magnetisation of which vanishes at a yet higher temperature. Such behaviour is not encountered in our samples.

We now turn back to the spectrum recorded for $x=1$ at 5 K and which seems to indicate a sudden increase of the HS fraction as soon as a static internal magnetic field is built up. The model of Bari and Sivardière and more detailed theoretical considerations by Sasaki and Kambara [31] have shown that strong magnetic fields shift the spin state equilibrium towards the HS state. According to the latter authors a field of 20 T is sufficient to cause a noticeable shift of $T_{1/2}$ towards lower temperatures. A field of 80 T allows to switch a LS compound to the HS state. The field dependence of the spin state equilibrium has been demonstrated experimentally by Qi et al. [32] although the field of 5 T induced only a weak shift of $T_{1/2}$ by -0.11 K. In the present case the static magnetic field in the spinel below T_N could be responsible for the crossover to the HS state of remaining LS–LS pairs so that only those Fe ions remain in the LS state which are exclusively surrounded by diamagnetic Ti(IV) ions. The residual

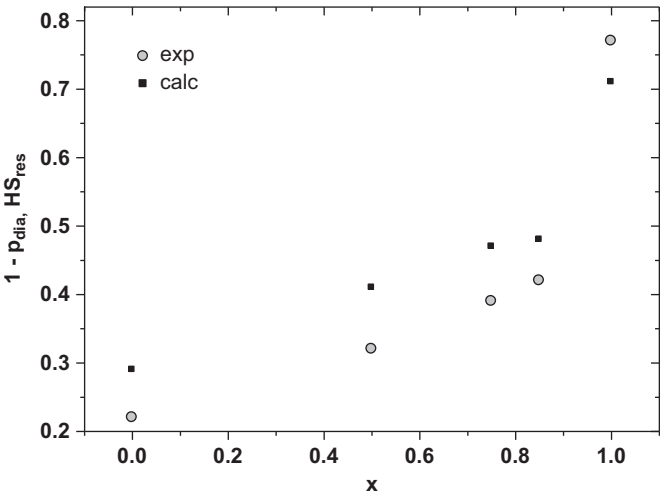

Fig. 12. Comparison of the residual HS fraction determined from Mössbauer spectra at 5 K (at 9 K for $x=0.85$, at 14 K for $x=1$) and the calculated probability $1-p_{dia}$ for an iron ion to be surrounded by at least one magnetic ion, both plotted versus *x*.

HS fraction of 84% from Mössbauer spectroscopy seems to be in good agreement with the value of 82% calculated above for such a case. This result is, however, to be considered with some caution. First, it has been shown that the transition from the paramagnetic to the antiferromagnetic state can be accompanied by an increase of the probability of recoil free γ-absorption [33] which would increase the spectral area of the HS state relative to that of LS iron. Second, the spectral areas at 5 K are rather uncertain due to the rather approximative nature of the fit of this spectrum. Further experimental work on this point is certainly needed for which spinel compounds seem to offer new and interesting opportunities.

5. Conclusion

The compound $CuFe_{0.5}Sn_{1.5}S_4$ is one of the rare examples where the energy difference between the high spin $3d(t_{2g})^4(e_g)^2$ and the low spin $3d(t_{2g})^6(e_g)^0$ electronic states of Fe(II) is of the order of kT in a spinel lattice. This situation makes $CuFe_{0.5}Sn_{1.5}S_4$ an ideal starting point for detailed investigations of the spin crossover phenomenon. The ease with which spinels form solid solutions with other spinel compounds by ion exchange offers interesting possibilities for the controlled variation of lattice properties with the aim of a controlled shift of the spin equilibrium.

In the present study the substitution of Sn(IV) by smaller Ti(IV) ions in the spinels $CuFe_{0.5}(Sn_{(1-x)}Ti_x)_{1.5}S_4$ $(0 \le x \le 1)$ allowed to obtain a closer packed crystal lattice by reduction of the lattice parameter a under conservation of the initial spinel structure. The closer packing enhances the antiferromagnetic spin–spin interaction between HS iron ions and leads to a spontaneous antiferromagnetic order at low temperatures for $x \ge 0.75$. The spin–spin interaction – only possible between neighbouring HS iron ions – reduces the free energy of the HS state with respect to the LS configuration and shifts the spin equilibrium towards the HS state. A correlation between the residual HS fraction and the probability to find magnetic neighbours around an iron ion is evidenced. Our results confirm predictions of model calculations by Bari and Sivardière on the influence of magnetic interactions on spin state equilibria. This study seems also to indicate that the internal magnetic field resulting from the static antiferromagnetic order in some samples further increases the HS fraction, in agreement with theoretical predictions.

The possibility to obtain strong internal magnetic fields by spin ordering – as demonstrated in the present study – might open new ways for the study of the influence of magnetic fields on spin state equilibria and might offer an alternative experimental approach as compared to the use of external fields and laboratory magnets.

Acknowledgment

The authors are grateful to R. Astier, Montpellier, for assistance in single crystal X-ray diffraction.

References

[1] Y. Tanabe, S. Sugano, J. Phys. Soc. Jpn. 9 (1954) 766–779.
[2] C.B. Bargeron, M. Avinor, H.G. Drickamer, Inorg. Chem. 10 (1971) 1338–1339.
[3] P. Gütlich, A. Hauser, H. Spiering, Angew. Chem. Int. Ed. Engl. 33 (1994) 2024–2054.
[4] P. Gütlich, Y. Garcia, H.A. Goodwin, Chem. Soc. Rev. 29 (2000) 419–427.
[5] J.A. Real, J. Zarembowitch, O. Kahn, X. Solans, Inorg. Chem. 26 (1987) 2939–2943.
[6] V. Ksenofontov, A.B. Gaspar, J.A. Real, P. Gütlich, J. Phys. Chem. B 105 (2001) 12266–12271.
[7] V. Ksenofontov, H. Spiering, S. Reiman, Y. Garcia, A.B. Gaspar, N. Moliner, J.A. Real, P. Gütlich, Chem. Phys. Lett. 348 (2001) 381–386.
[8] A. Simon, H.G. von Schnering, H. Schäfer, Z. Anorg. Allg. Chem. 355 (1967) 295–310.
[9] C.N.R. Rao, M.M. Seikh, C. Narayana, Top. Curr. Chem. 234 (2004) 1–21.
[10] M. Eibschütz, M.E. Lines, F.J. DiSalvo, Phys. Rev. B15 (1977) 103–114.
[11] M. Womes, J.C. Jumas, J. Olivier-Fourcade, F. Aubertin, U. Gonser, Chem. Phys. Lett. 201 (1993) 555–558.
[12] J. Padiou, J.C. Jumas, M. Ribes, Rev. Chim. Minér. 18 (1981) 33–42.
[13] J.C. Jumas, E. Philippot, M. Maurin, Acta Crystallogr. B35 (1979) 2195–2197.
[14] G. Springer, Miner. Mag. 36 (1968) 1045–1051.
[15] C. Branci, J. Sarradin, J. Olivier-Fourcade, J.C. Jumas, Mol. Cryst. Liq. Cryst. 311 (1998) 69–74.
[16] C. Branci, M. Womes, P.E. Lippens, J. Olivier-Fourcade, J.C. Jumas, J. Solid State Chem. 150 (2000) 363–370.
[17] H. Schäfer, H. Jacob, K. Etzel, Z. Anorg. Allg. Chem. 286 (1956) 27–41.
[18] R. Nitsche, H.U. Bölsterli, U. Lichtensteiger, J. Phys. Chem. Solids 21 (1961) 199–205.
[19] P. Lavela, C. Pérez-Vicente, J.L. Tirado, C. Branci, J. Olivier-Fourcade, J.C. Jumas, Chem. Mater. 11 (1999) 2687–2693.
[20] R.D. Shannon, Acta Crystallogr. A32 (1976) 751.
[21] N.N. Greenwood, T.C. Gibb, Mössbauer Spectroscopy, Chapman and Hall, London, 1971 (Chapter 8).
[22] Y. Maeda, N. Tsutsumi, Y. Takashima, Inorg. Chem. 23 (1984) 2440–2447.
[23] P. Adler, H. Spiering, P. Gütlich, J. Phys. Chem. Solids 50 (1989) 587–597.
[24] J.G. Leipoldt, P. Coppens, Inorg. Chem. 12 (1973) 2269–2274.
[25] S.K. Banerjee, W. O'Reilly, T.C. Gibb, N.N. Greenwood, J. Phys. Chem. Solids 28 (1967) 1323–1335.
[26] R. Ingalls, Phys. Rev. 133 (1964) A787–A797.
[27] J.B. Goodenough, Magnetism and the Chemical Bond, Interscience Publishers, New York, 1963.
[28] G.M. Bancroft, Mössbauer Spectroscopy. An Introduction for Inorganic Chemists and Geochemists, McGraw Hill, London, 1973.
[29] D.B. Chestnut, J. Chem. Phys. 40 (1964) 405–411.
[30] R.A. Bari, J. Sivardière, Phys. Rev. B 5 (1972) 4466–4471.
[31] N. Sasaki, T. Kambara, J. Phys. C: Solid State Phys. 15 (1982) 1035–1047.
[32] Y. Qi, E.W. Müller, H. Spiering, P. Gütlich, Chem. Phys. Lett. 101 (1983) 503–505.
[33] J.M.D. Coey, G.A. Sawatzky, A.H. Morrish, Phys. Rev. 184 (1969) 334–337.